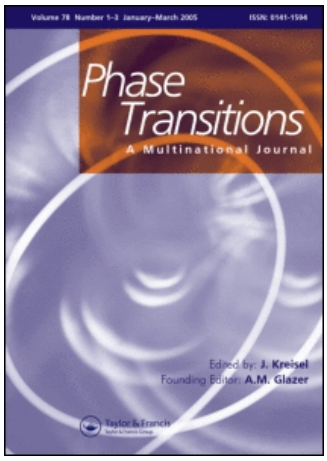

Phase Transitions
A Multinational Journal
Publication details, including instructions for authors and subscription information:
http://www.informaworld.com/smpp/title~content=t713647403

First principles calculations, crystal chemistry and properties of ferroelectric perovskites

To cite this Article: Grinberg, I. and Rappe, A. M. , 'First principles calculations, crystal chemistry and properties of ferroelectric perovskites', Phase Transitions, 80:4, 351 - 368
To link to this article: DOI: 10.1080/01411590701228505
URL: http://dx.doi.org/10.1080/01411590701228505

Phase Transitions,
Vol. 80, Nos. 4–5, April–May 2007, 351–368

First principles calculations, crystal chemistry and properties of ferroelectric perovskites

I. GRINBERG and A. M. RAPPE*

The Makineni Theoretical Laboratories, Department of Chemistry,
University of Pennsylvania, Philadelphia, PA 19104-6323, USA

(*Received 19 June 2006; in final form 19 April 2007*)

Using data obtained by *ab initio* calculations on a variety of ferroelectric (FE) perovskite solid solutions, we show that dependence of local structure of these complex materials on composition can be naturally understood in terms of crystal chemical concepts. Large supercell density functional theory calculations allow accurate description of interatomic interactions which can be directly linked to the technologically important macroscopic properties of the material through structure-property correlations. The obtained relationships between atomic characteristics and bulk solid-state behavior provide guidance for synthesis of next-generation ferroelectric materials.

Keywords: Ferroelectric perovskites; PZT; PMN-PT

1. Introduction

Ferroelectric (FE) perovskites have played an important role in technology for the past sixty years [1]. In particular, solid solutions such as $Pb(Zr,Ti)O_3$ (PZT) and $PbMg_{1.3}Nb_{2/3}O_3$–$PbTiO_3$ (PMN-PT) have exhibited superior properties [2]. These systems also exhibit a wealth of intriguing physical effects, making them interesting from a fundamental scientific point of view as well. In the 1990s, theoretical *ab initio* methods were first used to explain the origin of ferroelectricity and other properties of simple perovskites from a standpoint of condensed matter physics [3–9]. At the same time, experimental investigations using neutron scattering techniques showed that the local structure of the perovskite solid solutions used in device applications was quite disordered but similar for a series of technologically important materials [10, 11]. The lack of translational symmetry in these materials makes crystal-chemistry based thinking more natural for trying to understand the relationships between microscopic structure and macroscopic properties. Large supercell *ab initio* calculations and crystal chemical analysis are powerful tools for investigation of disordered perovskite ferroelectrics. In this article, we will review the efforts that our group has undertaken in this field [12–20] and will outline our current understanding of these complex materials.

*Corresponding author. Email: rappe@sas.upenn.edu

Phase Transitions
ISSN 0141-1594 print/ISSN 1029-0338 online © 2007 Taylor & Francis
http://www.tandf.co.uk/journals
DOI: 10.1080/01411590701228505

2. Methodology

2.1. *Computational method*

To directly model the quenched cation disorder in ferroelectric solid solutions and the local structural response to the cation arrangement, we use density functional theory (DFT) calculations on 40–60 atom supercells with a variety of cation arrangements. The supercells used in our calculations can be thought as a snapshots of small regions of the real disordered solid solution. To fully explore the potential energy surface, we start with atomic positions with fairly large (up to 0.4 Å) random distortions from the ideal perovskite positions. We then minimize the energy without imposing any symmetry constraints. This allows us to find low-symmetry ground states. More details about the computational methods can be found in previous publications [12–20]. The ground state ionic coordinates obtained in this way are quite accurate, as demonstrated by excellent agreement between experimental pair distribution functions PDF) obtained by neutron scattering and those predicted from DFT relaxed structures (figure 1).

2.2. *Crystal chemistry analysis*

In the crystal-chemistry approach, individual atoms are treated as distinct entities, which possess transferable properties, for example atomic size and displacement magnitude. In a complex oxide, optimal values for all atomic properties often cannot be achieved simultaneously, and the material assumes a compromise structure with tradeoffs among the various atoms. Once the relaxed structures are obtained, we analyze the behavior of each ion in terms of local structural motifs, analogous to the treatment of shell structures in liquids. Similar to a fluid, there are many different local configurations which give rise to the macroscopic properties of the material. Pair distribution functions provide statistical ensemble average information about interatomic distances even for completely aperiodic systems, and are thus a natural choice for analysis of local structure in disordered solid solutions. Examination of experimental PDFs (which are summed over all pairs of atoms) has provided crucial insights into the structure and dynamics of several materials [10, 11]. In our case, we have an additional advantage of being able to easily resolve the individual partial PDFs to provide additional information unavailable from experimental data.

The main crystal chemical concepts relevant to ferroelectric perovskites are ionic size, bond valence and the intrinsic displacement preference of the cation-oxygen complex (related to bond covalency). The values of these crystal chemical parameters for the cations typically found on the ferroelectric perovskite A- and B-sites are given in tables 1 and 2.

Ionic size is one of the oldest and simplest crystal-chemistry concepts. For each ion, Shannon and Prewitt assigned a particular ionic size, depending on the coordination number, which can then be used to predict bond lengths in the solid-state materials by adding the ionic radii of the two atoms involved in the bond [21]. Analysis of our DFT data showed that this concept works quite well for FE perovskite solutions, with an average bond length between a cation and an oxygen anion transferable between different materials. In the perovskite ABO_3 structure, the A–O and B–O sublattices have their own preferred bond lengths and lattice parameters. In some cases such as $PbTiO_3$, the preferences of the two sublattices nearly coincide, in other

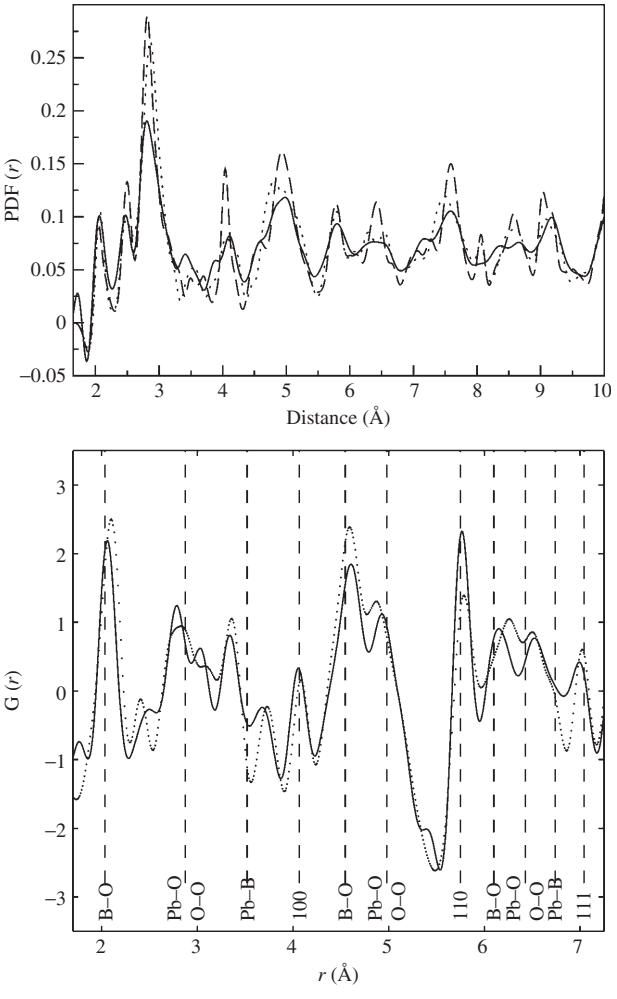

Figure 1. Comparison of experimental (solid) and theoretical (dotted for 60-atom, dashed for 40-atom) PDFs for PZT (above) and PSW (below) taken from Refs. [15] and [16]. Close agreement shows that DFT provides accurate description of the local structure.

Table 1. Values for crystal chemical parameters valence (V), ionic size (R) and ionic displacement (D^0) for A-site ions found in ferroelectric perovskites. Ionic size and displacements are in Å. Ionic size data taken from Ref. [21].

	V	R	D^0
K	1	1.64	0.05
Na	1	1.39	0.05
Ag	1	1.39	0.35
Ba	2	1.61	0.05
Pb	2	1.49	0.45
Sr	2	1.44	0.05
Ca	2	1.34	0.05
Cd	2	1.31	0.35
Bi	3	1.38	0.80
La	3	1.36	0.05

Table 2. Values for crystal chemical parameter valence (V), ionic size (R) and ionic displacement (D^0) for A-site ions found in FE perovskites. Ionic size and displacements are in Å . Ionic size data taken from Ref. [21].

	V	R	D^0
Cd	2	0.95	0.11
Mn	2	0.83	0.08
Zn	2	0.74	0.25
Mg	2	0.72	0.08
Ni	2	0.69	0.08
Yb	3	0.86	0.08
In	3	0.80	0.08
Sc	3	0.745	0.11
Fe	3	0.645	0.17
Mn	2	0.645	0.13
Zr	4	0.72	0.13
Hf	4	0.72	0.13
Ti	4	0.60	0.25
Nb	5	0.64	0.17
Ta	5	0.64	0.17
W	6	0.60	0.10

cases, the A–O sublattice would prefer either a shorter ($PbZrO_3$) or a longer ($BaTiO_3$) lattice constant than the B–O sublattice. In such cases, the actual lattice parameters assumed by the material are a compromise between the two preferences. To characterize the A–O/B–O competition in perovskites, the tolerance factor t is defined as

$$t = R_{A-O}/\sqrt{2}R_{B-O} \tag{1}$$

where R_{A-O} is the sum of A and O ionic radii and R_{B-O} is the sum of B and O ionic radii. Tolerance factor $t < 1$ leads to the rotation of the B–O_6 octahedra, accommodating the larger B–O sublattice by expansion of B–O_6 octahedra and accommodating the smaller A–O sublattice by shrinking the volume of the A-site. Such octahedral rotations often generate a low temperature antiferroelectric (AFE) phase (e.g., in $PbZrO_3$). If $t > 1$, the B–O_6 octahedra are stretched from their preferred B–O bond lengths, promoting B-cation distortions by creating room for the B-cations to off-center. Therefore, simple perovskites with $t > 1$ are usually ferroelectric. In the case of perovskites with mixed ion occupation on the B-site, the B–O_6 octahedra of the larger B cation will be larger than those of the smaller B-cation.

The concept of valence is quite old and has been found to apply to both ionic and covalently bonded materials. For oxides, empirically derived formulas have been used to quantify the relationship between the bond length and bond order [22]. Each atom has a desired valence (or total bond order) V_0. This is usually equal to the formal charge. The actual valence on each ion can be calculated as a sum of individual cation–anion bond orders which are expressed as a function of the bond distance R_{ij}. Using Brown's power law formulations, the deviation from the ideal valence $V_{i,0}$ for ion i is

$$\delta V_i = \Sigma_j (R_{ij}/R_{ij,0})^{-N_{ij}} - V_{ij,0} \tag{2}$$

The j sum runs over all nearest neighbors of the ith atom and R_{ij}^0 and N_{ij} are parameters relating bond strength to interatomic distance. Large deviation from ideal valence are energetically unfavorable, so that in the ground state structure all toms should have valence close to the ideal value. The preferences for total bond-order conservation gives rise to oxygen-mediated cation–cation repulsive interactions. The validity of this approach for FE perovskites has been confirmed by our analysis of ground state structures for a variety of atomic arrangements and compositions which found that atomic valence calculated by empirical formulas deviated by 0.05 on average from the ideal atomic valence [16].

In FE perovskites, the intrinsic preference of the cation to distort inside its oxygen complex (D^0) plays an important role. This property is related to the covalency of cation–oxygen bond. For example, Pb and Sr have essentially identical ionic size and are both +2 cations in perovskites. Yet, while $PbTiO_3$ is a classic ferroelectric material with strong ferroelectricity and T_c of 765 K, in $SrTiO_3$ the weak ferroelectric distortion is suppressed by zero-point fluctuations leading to a quantum paraelectric behavior [23]. This dramatic difference is due to the formation of covalent bonds due to the stereochemical active lone pair on the Pb atom [24, 25]. Such covalency is completely absent in $SrTiO_3$, where the simple metal Sr forms ionic bonds with the oxygen atoms. Thus, in ferroelectrics, the presence or absence of covalency manifest themselves in the magnitude of the preferred off-center distortion D_B^0, crucial for polarization of the material [3]. Examination of the 0 K DFT displacement data for a variety of ferroelectric solid solutions of $PbTiO_3$ showed that displacements for a particular B-cation in the tetragonal phase are similar among different solid solutions (figure 2), reflecting on average the intrinsic distortion preference of each B–O_6 complex. This allows us to assign D_B^0 values for B-cations typically present in FE perovskites (table 2). Our calculation results and data in the literature can be used to assign intrinsic distortion preference magnitudes (D_A^0) for the A-site cations as well (table 1).

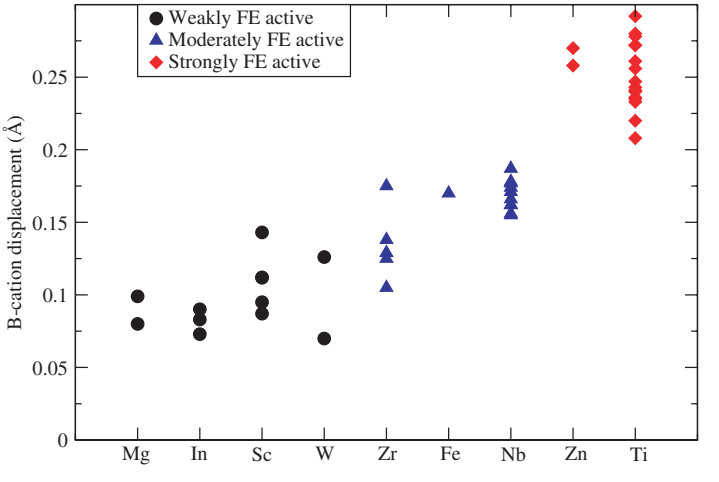

Figure 2. Distortion magnitudes (in Å) for B-cations in PT solid solutions. Distortion magnitudes are especially large for Zn and Ti. D_B values of 0.08, 0.07, 0.11, 0.10, 0.13, 0.17, 0.17, 0.25 and 0.25 Å are assigned for Mg, In, Sc, W, Zr, Fe, Nb, Zn and Ti respectively.

3. Local structure

Previous studies [3, 4] have shown that Pb-based ferroelectrics are A-site driven while such classic ferroelectric perovskites as $BaTiO_3$ and $KNbO_3$ are B-site driven. In $BaTiO_3$ and $KNbO_3$, the tolerance factor is quite large, t=1.06 and t=1.045 respectively. This means that in the ideal perovskite the B-site ion is underbonded, necessitating B-site off-centering which results in a spontaneous polarization. In contrast, first-principles calculations have shown that in the absence of Pb displacement, Ti distortion is unfavorable in $PbTiO_3$ [9]. The tolerance factor of $PbTiO_3$ (1.02) is more similar to that of the $SrTiO_3$ material which displays only small B-site distortions [23]. Thus, the creation of ferroelectricity in $PbTiO_3$ requires a strong displacements by the A-site Pb ion which is due to the strong preference of Pb to form short, covalent Pb–O bonds.

In a solid solution, Pb atoms are more sensitive to the perturbations created by B-cation disorder than the B-cations. This is due to the fact that the anisotropy created by the disordered B-cation arrangement is stronger for the Pb local environment than for the B-cation environment. In the ideal perovskite structure, both Pb and B-cations have a symmetrical nearest-neighbor oxygen shell. For Pb, symmetry is broken in the second-nearest neighbor shell formed by the B-cations in a disordered arrangement. For the B-cations the second-nearest neighbor shell is formed by identical Pb atoms and Zr/Ti disorder breaks symmetry in the third-nearest neighbor shell. The A-site ions are also more flexible and more responsive than the B-cations. This is due to the weaker bonds between Pb and O (average bond order of 1/6) as opposed to Ti and O (average bond order 2/3). Taken together, this means that the B-cations are insensitive to local differences in B-cation arrangement and will only respond to large forces, generated by the overall direction of polarization. In a solid solution, this will lead to a narrow distribution of B-site distortion directions. In contrast, due to their greater sensitivity and flexibility Pb ions will exhibit a more broad distribution and will determine a compromise overall direction of polarization (figure 3). Thus the response of Pb distortions to B-cation arrangement and composition will be the crucial factor in determining the direction of overall polarization of the material.

3.1. *The influence of ionic size — PZT*

Our work has elucidated the role of ionic size differences in determining the local structure in solid solutions. A larger size of the B-cations leads to an increased repulsion between the positively charged Pb ions and B-cations. This effect can be clearly observed by examination of the local structure of the 50/50 PZT (figure 4), where Pb ions distort away from the larger Zr ions and toward the smaller Ti ions. Similarly, analysis of the Pb–Zr and Pb–Ti distances in the relaxed structure shows (figure 5) that the first peak of Pb–Zr partial PDF is located at larger distance than the first peak in the Pb–Ti PDF, with the 0.1 Å separation between the two peaks consistent with the difference between the Zr^{4+} and Ti^{4+} ionic radii (0.12 Å). Introducing a quenched disorder in the B-cation arrangement for B-cations of different sizes gives rise to anisotropy in the local short-range repulsive potential felt by the Pb cations and leads to a disordered local structure with a distribution of cation distortion directions around the overall polarization direction.

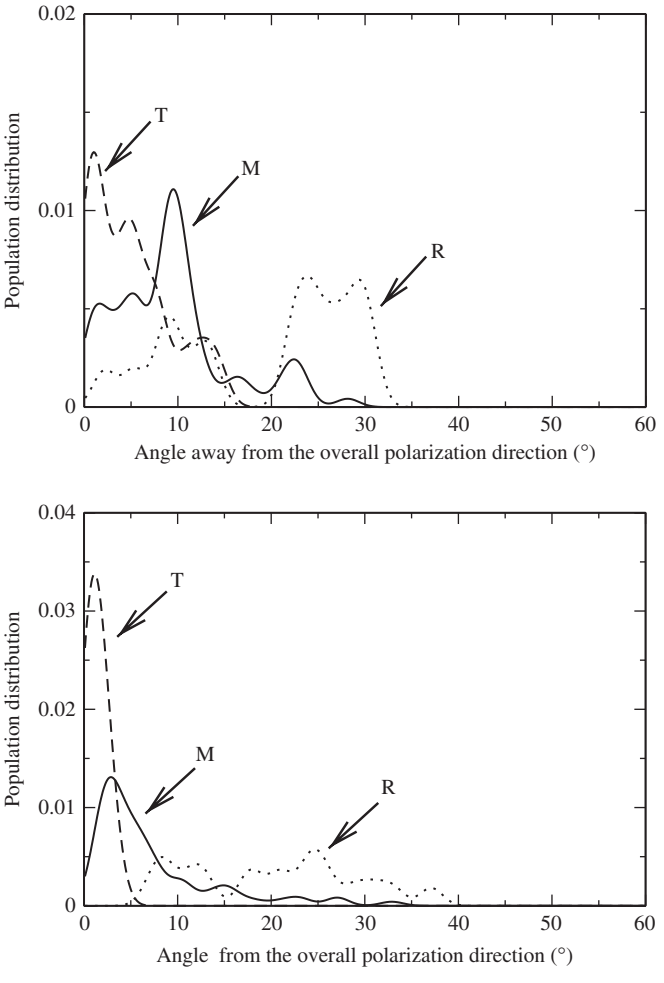

Figure 3. Distribution of Pb (above) and B-cation (below) distortion angles away from overall polarization direction of the supercell for T (dashed), M (solid) and R (dotted) PZT.

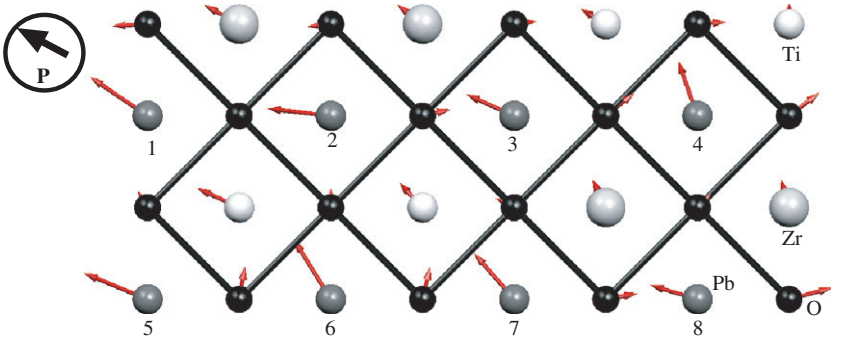

Figure 4. Projection of the DFT relaxed structure for $4 \times 2 \times 1$ 50/50 PZT supercell on the $x - y$ plane. Pb atoms tend to distort away from the large Zr and toward smaller Ti cations.

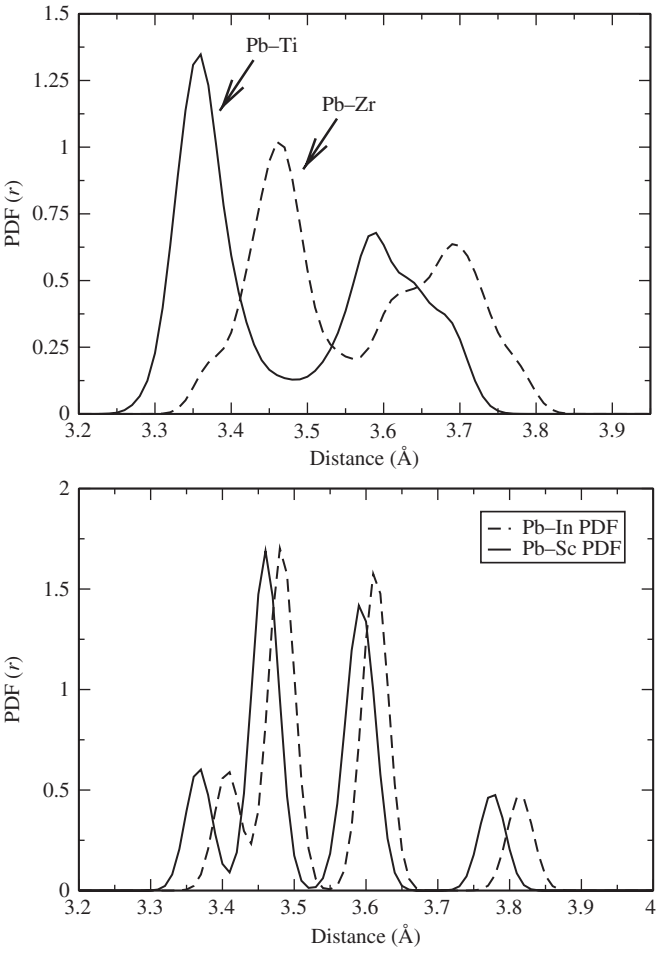

Figure 5. Pb–B-cation partial PDFs. (above) Pb–Ti (solid) and Pb–Zr (dashed) partial PDFs obtained from the relaxed structures of the 50/50 PZT supercells at experimental lattice constants. (below) Pb–Sc (solid) and Pb–In (dashed) partial PDFs obtained from the relaxed structures of $PbSc_{1/2}N_{1/2}O_3$ and $PbIn_{1/2}N_{1/2}O_3$ at experimental lattice constants.

Our investigations have shown how the interplay of the dipole interactions and local A–B cation repulsion gives rise to structural phases transitions such as the morphotropic phase boundary (MPB) between the rhombohedral (R) and tetragonal (T) phases present at 50/50 Zr/Ti composition [14]. The Pb distortions are produced by several interactions. In all PZT phases, Pb tends to move toward (100), (010), and (001) faces in order to form stronger bonds with four of its oxygen neighbors, without closely encountering B cations. Each Pb has a choice of six such faces. The Pb atoms also tend to move toward the face that is closest to the overall polarization direction in order to lower the dipole interaction energy. If this face is Ti-rich (0 or 1 Zr), the Pb will move toward it strongly (perhaps with a small tilt away from the Zr). A neutral face (2 Zr and 2 Ti) permits moderate Pb motion toward it, with a significant tilt. Zr-rich (3 or 4 Zr) faces cause the Pb to tend to move toward a different face to avoid large Pb–Zr repulsion.

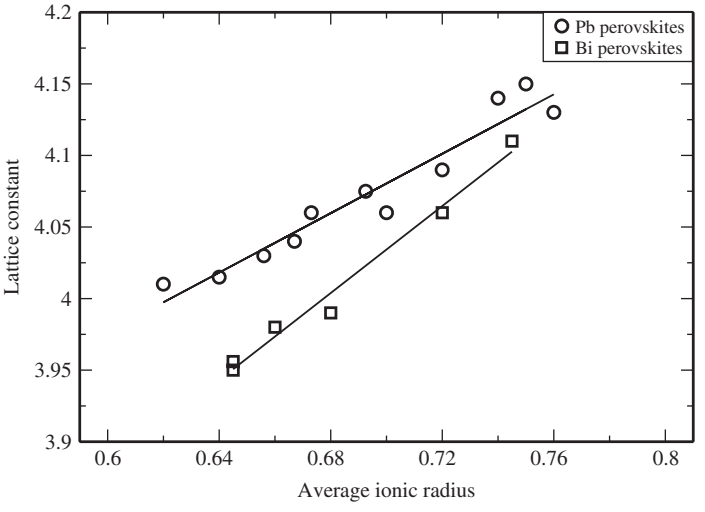

Figure 6. Lattice constant (volume$^{1/3}$) in Pb- and Bi-based FE perovskites *vs.* average B-cation size. The increase in ionic size is not fully accomodated by the increase in solid-state cell parameters.

In the Ti-rich region of the phase diagram, Ti-rich faces dominate and a T phase (with Pb distortions aligning in one direction) minimizes the dipole alignment energy without raising the repulsion energy. The R phase, with Pb distortions in a variety of directions, minimizes the local repulsion energy just as well as the T phase but results in a larger dipole interaction energy cost. Therefore the T phase is preferred. In the Zr-rich region of the phase diagram, Zr-rich faces dominate and T Pb distortions with small angle scatter can minimize the dipole interaction energy only by suffering a high A–B repulsion energy cost. Therefore the R phase is preferred. Here, the Pb atoms distort in a variety of directions toward the available Ti-rich faces to reduce local repulsion cost. However, this large variation in distortion direction raises the dipole interaction energy. Unlike the Ti-rich T phase, the Zr-rich R phase is a disordered compromise structure where trade-offs are made between the two components of the energy. This explains the difference in angle scatter at various compositions of PZT found by DFT calculations.

At around 50/50 composition, equal amounts of Zr-rich, Ti-rich and neutral faces are present in the material. A concerted distortion in a tetragonal direction can be accommodated by the Pb atoms encountering a Ti-rich or a neutral face. However, the Pb atoms encountering a Zr-rich face must distort in other directions to minimize the A–B repulsion, creating a (211) polarization of the monoclinic phase.

Increasing ionic size of the B-site cations can be thought of as a crystal chemical way to simulate high pressure. Application of external pressure decreases interatomic distances in the material, increasing the interatomic repulsions. In ferroelectrics, these effects are also produced by substitution of large ions on the perovskite B-site. The most obvious effect of B-site compositional changes in perovskite solid solutions is the change in the volume of the material. Figure 6 shows that there is a clear linear correlation between the average B-cation ionic size and perovskite lattice constant (volume$^{1/3}$) for a range of Pb-based and Bi-based perovskites.

At first glance, the increased volume due to increased ionic size should simulate the effects of negative pressure. However, a closer inspection of the trend for Pb-based perovskites in figure 6 shows that the slope of lattice constant versus ionic radius is about 1.0, so that a 0.1 Å increase in the average ionic radius induces an increase in lattice constant of 0.1 Å. However, since two B–O bond lengths are present along a Cartesian direction of the perovskite unit cell, a 0.2 Å lattice expansion (or a 2.0 slope in the trend in figure 6) is necessary to fully accommodate the larger size of the B-cation. The smaller slope in figure 6 indicates that the B–O_6 cages are compressed from their ideal size by the compromise with the Pb–O sublattice which favors shorter bond lengths. A larger mismatch between the preferred bond distances of the two sublattices, corresponding to a lower tolerance factor, generates larger pressure on the B–O_6 cage. The stronger repulsive interactions due to larger size of the B-site cation also reduce the free volume of the A-site. This explains why increasing the content of the larger Zr ion in PZT solution (which raises the volume) has the same effects on properties as increasing external pressure on the $PbTiO_3$ end-member as found by recent calculations of Wu and Cohen [26].

3.2. *The influence of ionic valence – heterovalent Perovskites*

The appearance of relaxor behavior and B-site ordering are the most important effects of the heterovalency on the B-site. The work of Davies and co-workers has demonstrated that B-site valence difference augmented by B-site ionic size difference results in ordered B-site arrangement in Pb-based perovskite [27, 28]. In $PbB^{3+}B^{5+}O_3$ and $PbB^{2+}B^{6+}O_3$ perovskites, perfect rocksalt ordering is found. In $PbB^{2+}B^{5+}O_3$ and $PbB^{2+}B^{6+}O_3$ perovskites, a random-site arrangement is preferred with one rocksalt site fully occupied by the majority B-site ion ($B^{5+}$for $PbB^{2+}_{1/3}B^{5+}_{2/3}O_3$ and B^{3+} for $PbB^{3+}_{2/3}B^{6+}_{1/3}O_3$) and the other occupied by the mixture of the majority and the minority B-cations. In the case of perfect rocksalt ordering, either FE or AFE behavior is observed. However, in the presence of disorder, heterovalency on the B-site leads to relaxor behavior.

We find that local arrangement of heterovalent B-cations has a strong effect on the directions of Pb distortions. Inspection of the relaxed structure of a 60-atom $PbMg_{1.3}Nb_{2/3}O_3$ (PMN) supercell (figure 7) shows that the location of Mg atoms is the primary influence on the direction of Pb distortions. In all cases Pb atoms avoid cube faces with three Nb atoms and one Mg atom and move toward cube faces with two Mg and two Nb atoms. The avoidance of Nb-rich faces is due to the presence of oxygen atom with two Nb neighbors. Such oxygen atoms have higher B–O bond order than the oxygen atoms in $PbTiO_3$ due to the higher valence of Nb. Since the total bond order of cation–oxygen bonds is conserved at 2, this prohibits the formation of short Pb–O bonds of high bond order and creates a strong effective Pb–Nb repulsive interaction. On the other hand, the oxygen atoms with Mg and Nb neighbors have a lower total B–O bond order than the oxygen atoms in $PbTiO_3$, necessitating a formation of more short Pb–O bonds to compensate for B–O bond depletion and leading to an attractive oxygen-mediated Pb–Mg interaction. The high anisotropy created by a large amount of highly overbonded and underbonded oxygen atoms [29] forbids the formation of a long-range ferroelectric state and leads to a relaxor phase. The ability of such short-range interactions to smear out the phase transition has been shown in an Ising model study by Fisch [30].

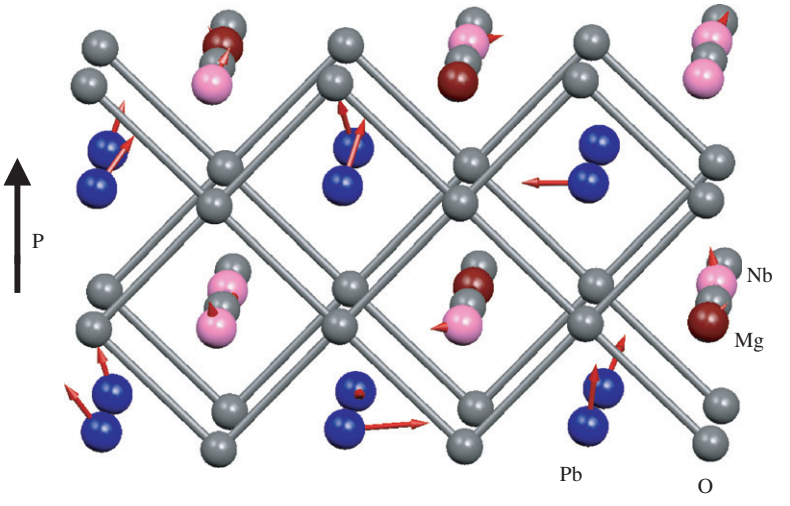

Figure 7. Relaxed structure of 60-atom supercell of PMN obtained by DFT calculations. Cation displacements from high-symmetry positions are shown by arrows scaled up by a factor of 4. Pb atoms displace away from Nb-rich faces. Blue, pink, red and gray represent Pb, Nb, Mg and O atoms respectively.

Investigations of $PbSc_{2/3}W_{1/3}O_3$–$PbTiO_3$ (PSW-PT) and $PbSc_{2/3}W_{1/3}O_3$–$PbZrO_3$ (PSW-PZ) solid solutions have shown how the local structure and transition temperature T_c of heterovalent solid solutions can be manipulated by variation in the B-cation ordering [16, 31].

Addition of up to 0.25 fraction of PT to random-site ordered PSW relaxor preserves the random-site order on the B-site with all Ti atoms replacing Sc atoms on the mixed site. Counterintuitively, despite the addition of high T_c PT, there is a decrease in the T_c (or the temperature maximum of the dielectric constant $T_{\epsilon,\max}$) (figure 8). In the PSW-25PT system, a rocksalt B-cation ordering is achieved with one half of the B-sites occupied by Sc atoms and the other half by a 50/50 mixture of W and Ti ions. Subsequent addition of PT results in Ti occupation of both sites and a rapid loss of B-site order. This is accompanied by a large increase in $T_{\epsilon,\max}$. In contrast, for PSW-PZ solution, a disruption of B-cation order and an increase in $T_{\epsilon,\max}$ are found in for all PZ concentrations.

To investigate the origins of the unusual non-monotonic compositional T_c trends in the PSW-PT solution, we investigated the local structure in PSW-PT using DFT calculations. We found that that in ordered PSW-PT, Pb and B-cation displacements are actually smaller than in pure PSW [16]. On the other hand, PSW-62.5PT, PSW-25PZ and PSW-62.5PZ all displayed larger cation displacements than the end-member PSW.

The weaker ferroelectricity in PSW-25PT is due to its rocksalt ordered B-cation arrangement. Here, each Ti ion is surrounded by six Sc ions. Due to their large size, in a variety of perovskite materials Sc ions have been found to makes only small distortions [20]. A large Ti distortion and formation of short, high bond-order Ti–O bonds without a large off-centering by the Sc ion leads to oxygen atom overbonding and is unfavorable. The unfavorable Ti–Sc distortion coupling suppresses Ti displacements leading to weaker ferroelectricity and lower T_c. In contrast to PSW-PT for $x < 0.25$, for all PSW-PZ compositions and for PSW-PT compositions with

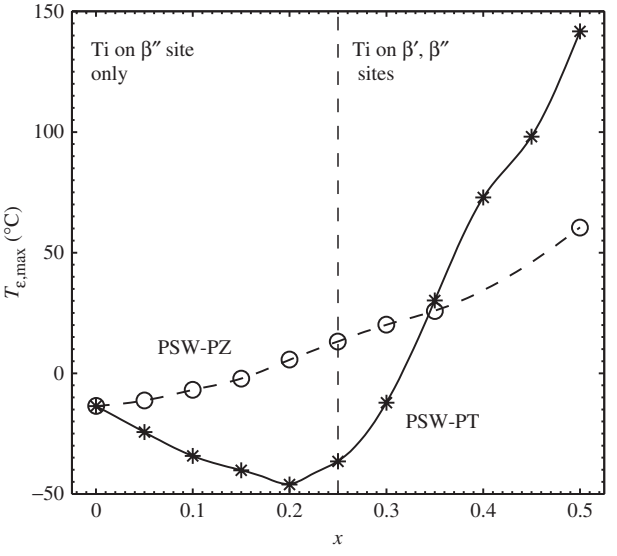

Figure 8. Evolution of $T_{\epsilon,\max}$ with composition in PSW-PT* and PSW-PZ° solid solutions [16, 29]. The non-linearity in PSW-PT system is due to suppression of B-cation displacement coupling due to B-site order.

$x > 0.25$, the B-cation arrangement is disordered. This enables coupling between Ti, Zr and W ions, leading to increase in cation distortions and T_c.

3.3. *The influence of ionic covalency*

In addition to traditional crystal chemical concepts of ionic size and valence, the electronic structure of the ions plays a crucial role in determining the local structure and properties in ferroelectric solid solutions. This was first explained by Cohen in his landmark paper on the classic ferroelectrics PT and $BaTiO_3$ (BT), where he showed that the much larger off-centering and ferroelectric instability of PT as compared to BT was directly related to hybridization of the Pb 6*s*6*p* and Ti 3*d* orbitals and the formation of the covalent Pb–O and Ti–O bonds [3]. Our recent studies found that differences in bonding character are responsible for the differences in bulk properties of ferroelectrics with Mg and Zn on the perovskite B-site [17].

Despite similar ionic size (0.72 Å for Mg and 0.74 Å for Zn) and valence of the B^{2+} ions, $PbZn_{1.3}Nb_{2/3}O_3$ (PZN) exhibits a higher $T_{\epsilon,\max}$ and larger dielectric constant than PMN. Comparison of PMN-PT and PZN-PT solid solutions shows that relaxor to rhombohedral ferroelectric and rhombohedral-tetragonal morophotropic phase boundary (MPB) transitions take place at much smaller PT content in PZN-PT than PMN-PT. Analysis of relaxed structures for several compositions in PMN-PT and PZN-PT solid solutions shows that for both solid solutions Pb displacement magnitudes (table 3) are unchanged by the addition of PT, whereas the average magnitude of the B-cation displacements steadily increases with PT content. The cation displacements are larger in PZN-PT than in PMN-PT, with especially large difference for the B^{2+} cations. While Mg ions are only slightly displaced, the Zn ions exhibit significant distortions even in pure PZN and Ti-like 0.27 Å distortions in Ti-rich PZN-PT. The larger Pb and Nb displacements in the PZN-PT system are due to the coupling between Zn and Pb and Nb off-center

Table 3. Results of DFT calculations for PMN-PT and PZN-PT systems. Predicted cation displacements from center of oxygen cage in Å, Pb displacement angle scatter $\theta_{\mathrm{Pb\ in^{\circ}}}$, average and local polarization in $\mathrm{C\,m^{-2}}$ and experimental $T_{\epsilon,\max}$ in K.

	Pb disp.	B^{2+} disp.	Nb/Ti disp.	θ_{Pb}	P_0 avg, loc	$T_{\epsilon,\max}$ exp.
PMN	0.398	0.056	0.168	65	0.38, 0.67	276
PMN-0.25PT	0.389	0.080	0.181	33	0.55, 0.68	397
PMN-0.625PT	0.387	0.099	0.216	28	0.66, 0.74	583
PT	0.440		0.280	0	0.88, 0.88	765
PZN	0.444	0.148	0.189	67	0.43, 0.73	424
PZN-0.25PT	0.461	0.258	0.205	35	0.66, 0.79	547
PZN-0.625PT	0.424	0.270	0.237	27	0.74, 0.80	643
PT	0.440		0.280	0	0.88, 0.88	765

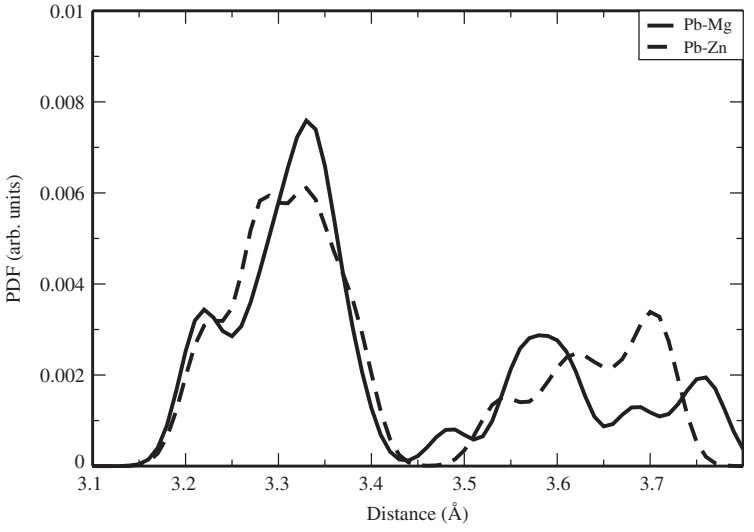

Figure 9. Partial Pb–B^{2+}-cation PDFs in PMN and PZN obtained from 60-atom PMN and PZN DFT supercell relaxed structures. Due to similar ionic size of Mg and Zn, first peaks of Pb–Zn and Pb–Mg PDFs are located at the same distance.

displacements through the Pb–B-cation repulsive interactions. The ionic size of Mg and Zn atoms is essentially the same, which leads to the same shortest allowed Pb–Mg and Pb–Zn distances (figure 9). The greater ability of Zn atoms to off-center allows Pb atoms in PZN-PT solution to preserve the required Pb–B-cation distances for larger Pb displacements than in the PMN-PT system. The larger Pb displacements in turn cause larger Nb and Ti distortions.

Large Zn distortions soften Pb–Zn repulsion, making perovskite faces with Zn atoms more friendly toward a Pb distortion than the corresponding perovskite faces with Mg atoms in PMN. This increases the population of the local environments favorable to tetragonal distortion, moving the relaxor to ferroelectric transition and the MPB to lower Ti concentrations. Larger cation distortions in PZN also lead to higher $T_{\epsilon,\max}$ in PZN than in PMN in accordance with the cation shift-T_c relationship (see below). The contrast between the absence of Mg off-centering and the large Zn displacements is due to the different electronic structure of the two

ions. While Mg is a simple metal and Mg^{2+}–O bonding is essentially ionic, the imperfect screening of the nuclear charge by the *d*-electrons and the presence of low-lying *p* orbitals make Zn more polarizable and enable covalent bonding with oxygen atoms. This means that covalent Zn–O bonding and large Zn distortions will be present in other perovskite systems. This has been confirmed recently by studies on the anomalous properties in $BiZn_{1/2}Ti_{1/2}O_3$-PT solid solution [32].

4. Structure–property correlations

A detailed database of structural information assembled for a range of ferroelectric solid solutions [14–20] has allowed us to quantify the arguments in the previous section, obtaining accurate predictors of transition temperatures and MPB locations.

4.1. *Predicting transition temperatures*

In 1968, Abrahams, Kurtz and Jamieson noted a correlation between cation shifts and transition temperatures for a variety of ferroelectrics. However, their relationship was only qualitatively accurate, with especially large discrepancies between predicted and experimental T_c values for the Pb containing perovskites $PbFe_{1/2}Nb_{1/2}O_3$ and PT.

Limiting ourselves to Pb-based A-site driven ferroelectrics, we find that there is also a strong relationship between the low-temperature cation displacements as found by our DFT calculations and the experimentally obtained temperature position of the dielectric constant maximum $T_{\epsilon,\max}$, with $T_{\epsilon,\max}$ at 1 MHz for PMN-PT, PZN-PT, PZT, $PbSc_{1/2}Nb_{1/2}O_3$ (PSN), PSW-PT and PSW-PZ solid solutions is predicted by

$$T_{\epsilon,\max} = aD_{\mathrm{Pb}}^2 + bD_{\mathrm{B}'}^2 f_{\mathrm{B}'}, \tag{3}$$

where D_{Pb} is the average magnitude of the Pb distortions, $D_{\mathrm{B}'}$ is the average magnitude of the distortions, $f_{\mathrm{B}'}$' is the fraction of the ferroelectrically active B-cations in solution and *a* and *b* are constants (1739 and 5961 respectively) in units of $\mathrm{K/\AA^2}$. The dependence of $T_{\epsilon,\max}$ on local structure presented in equation (3) can be further simplified by transforming cation and oxygen displacements into 0 K local dipole moments via multiplication by their Born effective charges. This leads to

$$T_{\epsilon,\max} = \gamma P_{\mathrm{loc}}^2, \tag{4}$$

$$T_{\epsilon,\max} = \gamma P_{\mathrm{avg}}^2 \tag{5}$$

where γ is a constant, P_{loc} and P_{avg} are the 0 K average magnitude of the local dipole moment and the overall polarization respectively. Figure 10 shows the correlation between the $T_{\epsilon,\max}$ predicted by equations (3) and (4) and experimental $T_{\epsilon,\max}$ data. The clustering of the data around the $y = x$ line indicates that equations (3) and (4) accurately and quantitatively capture the trends in $T_{\epsilon,\max}$ among these fairly different systems. Comparing the data for PMN-PT and PZN-PT systems in table 1, we see that the higher $T_{\epsilon,\max}$ for PZN-PT system is directly related to larger P_{loc} and P_{avg} values due to off-centering behavior on the B^{2+} site.

The nearly constant dependence of $T_{\epsilon,\max}$ on P_{loc} and P_{avg} can be interpreted as follows. Experimental results have shown that ferroelectric to paraelectric phase transitions in Pb based perovskites such as PMN and PZT are of order-disorder character, with Pb displacements at T_0 of up to 70% of the low temperature

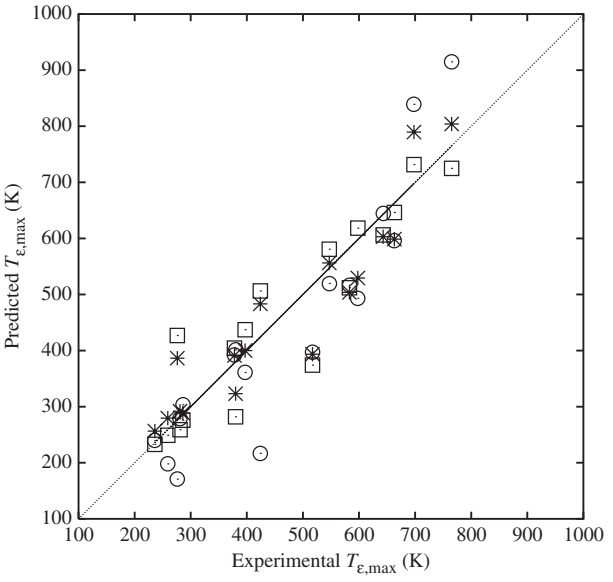

Figure 10. Correlations between experimental $T_{\epsilon,\max}$ and predicted $T_{\epsilon,\max}$ for PZN, PZN-2PT, PMN, PMN-PT, PSW, PSW-PT, PSW-PZ, PSN and PZT systems. Values for predicted $T_{\epsilon,\max}$ are obtained by equation (3) (squares) with $a = 1739$ and $b = 5961$, equation (4) using local polarization with $\gamma = 942$ (stars) and equation (5) using overall polarization with $\gamma = 1189$ (circles).

value [34]. The parameter governing the temperature of such an order-disorder transition is the coupling strength between the Pb and B-cation displacements in neighboring unit cells (corresponding to the J parameter in spin models). The coupling is due to electrostatic effects favoring dipole alignment and covalent chemical bonding effects disfavoring under- and over-bonded oxygen atoms. Dipole alignment strengths depend only on polarization strengths and gives rise to the overall dependence of T_c on square of polarization, with the variation in through-oxygen coupling accounting for the differences between experimental and predicted $T_{\epsilon,\max}$ values in figure 10.

4.2. *Predicting MPB locations*

The search for new piezoelectrics has been hindered by the lack of guidance on likely MPB compositions. This necessitates time-consuming experimental synthesis for a range of compositions to locate the MPB and to determine the properties of interest. Recently, we have shown that by taking into account the off-centering tendencies of the B-cations as revealed by DFT calculations, a highly accurate predictive relationship between properties of the constituent ions and the PT content at MPB of $PbTiO_3$ based solid solutions ($x_{PT,MPB}$) can be obtained to guide future synthesis efforts [20].

The mechanism for MPB formation described in section 3.1 implies that a solid solution of PT and a perovskite with a larger size B-cation such as $PbYb_{1/2}Nb_{1/2}O_3$ (PYN) (average B-cation size of 0.754 Å *versus* 0.72 Å for Zr) will have an MPB at higher PT content due to stronger Pb–B-cation repulsion and a large energy cost of collinear (100) displacements. Conversely, a solid solution of PT and a perovskite

with a smaller size B-cations such as PMN (average B-cation size of 0.67 Å *versus* 0.72 Å for Zr) will have an MPB at lower PT content due to weaker Pb–B-cation repulsion. (In the following arguments, we ignore the influence of indirect through-oxygen Pb–B-cation repulsions. While these interactions are important in ordered systems such as PMN and PZN, we expect that that under-bonding and overbonding induced by the presence of heterovalent cations on the B-site will average out for compositions relevant to this work, due to destruction of B-cation order by Ti substitution at low PT content.) Similarities between Bi and Pb behavior on the perovskite A-site mean that this mechanism will not be fundamentally changed by the presence of Bi ions on the A-site. We quantify these arguments by

$$\Delta E_{\mathrm{T-R}}(x_{\mathrm{nPT}}) = -\Delta E_{\mathrm{dis}}(x_{\mathrm{nPT}}) + \Delta E_{\mathrm{A-B}}(x_{\mathrm{nPT}}) \tag{6}$$

where $\Delta E_{\mathrm{T-R}}$ is the energy difference between the T and R phases, x_{nPT} is the fraction of the non-PT end member in the solid solution, ΔE_{dis} is the energy cost of disordering the cation displacements due to electrostatic and bonding interaction and $\Delta E_{\mathrm{A-B}}$ is the energy cost due to A–B repulsion incurred by collinear (100) cation displacements of Pb and Bi ions. The MPB is located at x_{nPT} such that $\Delta E_{\mathrm{T-R}}$ is 0 and $\Delta E_{\mathrm{dis}}=\Delta E_{\mathrm{A-B}}$. Since Pb displacements in the tetragonal phase of PT solid solutions are fairly similar, we can make a zeroth-order approximation that $\Delta E_{\mathrm{dis}}(x_{\mathrm{nPT}})$ is independent of composition and is constant for all systems. Although this approximation is rather crude, it turns out to be valid for reproducing experimental observations.

As a first approximation, we take the A–B repulsion to be a linear function of the ionic size of the B-cation and the A–B interatomic distance. The dependence of the $\Delta E_{\mathrm{A-B}}(x_{\mathrm{nPT}})$ on ionic size is intuitive – larger ions give rise to stronger interatomic repulsions. A large ionic size of the B-cation usually makes B-cation displacements unfavorable (rattling cation model), giving rise to larger indirect repulsion contributions as well. Since Pb displacements in the tetragonal phase and the perovskite volume are fairly constant for a wide variety of PT solid solutions, the Pb–B interatomic distance will be also a linear function of the B-cation displacement D_{B}. Analysis of Bi–B-cation distances shows that the dependence of Bi–B-cation repulsion on ionic size and displacement of the B-cation will not be too different from the case of Pb–B-cation repulsive interactions. At the MPB, R and T phase energies are equal and

$$\begin{aligned} &x_{\mathrm{nPT}}(a_0 + b_0 R_{\mathrm{B,\,avg}} - c_0 D_{\mathrm{B,\,avg}}) + (1 - x_{\mathrm{nPT}})(a_0 + b_0 R_{\mathrm{Ti}} - c_0 D_{\mathrm{Ti}}) \\ &\quad - \Delta E_{\mathrm{dis}}(x_{\mathrm{nPT}}) = 0 \end{aligned} \tag{7}$$

We now solve for x_{nPT}, set the numerator to 1 and collect all terms that do not depend on the identity of non-PT end member. Using new constants a_1, b_1 and c_1, and the fact that $x_{\mathrm{PT}} = 1 - x_{\mathrm{nPT}}$ we get

$$x_{\mathrm{PT,\,MPB}} = 1 - 1/(a_1 + b_1 R_{\mathrm{B,\,avg}} - c_1 D_{\mathrm{B,\,avg}}). \tag{8}$$

Using R_{B} and D_{B} values for solid solutions containing elements for which we have DFT D_{B} data, we fit the experimentally observed PT content at MPB to equation (8). For Pb-based solid solutions we obtain 0.34, 3.31 and 7.49 as values for a_1, b_1 and c_1 constants. For solid solutions with mixed Pb and Bi occupation of the A-site, our fit a_1, b_1 and c_1 values are $-0.97, 5.71$ and 7.69. The correlation between the $x_{\mathrm{PT,\,MPB}}$ values predicted by the fits and observed experimentally is shown in figure 11.

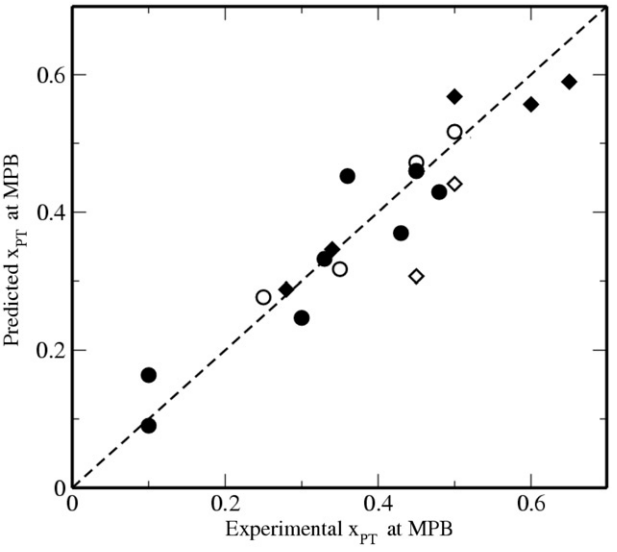

Figure 11. Correlation between the mole fractions of PT at MPB predicted by equation (8) using data in table 3 and mole fractions of PT at MPB observed experimentally. Solid solutions for which we have DFT B-cation displacement data are marked by filled cirles and diamonds for Pb-based and Bi-based systems respectively. MPB positions predicted for Pb- and Bi-based systems where B-cation displacement data is estimated are marked by open circles and diamonds respectively.

All predicted PT mole fractions are within 0.15 for the end members with B-cations for which we have DFT displacement data.

5. Future outlook

Despite the progress in understanding the physics of complex ferroelectric systems, several unsolved problems remain. Behavior of these materials at nanoscale dimension in thin-films and nanowires has recently received much attention [35], with fascinating new physics and properties discovered at the oxide-metal [36] and oxide-gas interface [37, 38]. Similarly, epitaxial strain and growth of heterostructures is promising for engineering material properties [39]. Molecular dynamics simulations of ferroelectrics are still in the beginning stage and will be crucial for obtaining detailed theoretical understanding of local structure and properties at domain walls and grain boundaries, important for NVRAM devices and single-crystal growth, for example. In further studies of bulk ferroelectrics, application of current understanding to materials design of new high-temperature, high-piezoelectric performance materials is of obvious interest. There is an especially strong interest in obtaining environmentally friendly lead free materials; theoretical efforts can play a crucial role in this research. In more fundamental research, quantitative understanding of relaxor behavior is still lacking, despite intense efforts. The recent increase in computational power is finally enabling accurate first-principles studies of realistic models for relaxor materials. Theoretical *ab initio* studies will surely make crucial contributions to future progress in the science of ferroelectrics.

Acknowledgements

We thank P. K. Davies for discussions about crystal chemistry. This work was supported by the Office of Naval Research under Grant No. N-00014-00-1-0372. Computational support was provided by the Center for Piezolectrics by Design, the DoD HPCMO, DURIP and by the NSF CRIF program, Grant No. CHE-0131132.

References

[1] M.E. Lines and A.M. Glass, *Principles and Applications of Ferroelectrics and Related Materials* (Clarendon Press, Oxford, 1977).
[2] S.-E. Park and T.R. Shrout, J. Appl. Phys. **82** 1804 (1997).
[3] R.E. Cohen, Nature **358** 136 (1992).
[4] W. Zhong, D. Vanderbilt and K.M. Rabe, Phys. Rev. Lett. **73** 1861 (1994).
[5] R. Yu and H. Krakauer, Phys. Rev. Lett. **74** 4067 (1995).
[6] D.J. Singh, Phys. Rev. B **52** 12559 (1995).
[7] L. Bellaiche, A. Garcia and D. Vanderbilt, Phys. Rev. Lett. **84**, 5427 (2000).
[8] H. Fu and R.E. Cohen, Nature **402**, 281 (2000).
[9] Ph. Ghosez, E. Cockayne, U.V. Waghmare, *et al*., Phys. Rev. B. **60** 836 (1999).
[10] T. Egami, W. Dmowski, M. Akbas, *et al*., First-Principles Calculations for Ferroelectrics—Fifth Williamsburg Workshop, edited by R.E. Cohen (American Institute of Physics, Melville, New York, 1998).
[11] I.-K. Jeong, T.W. Darling, J.K. Lee, *et al*., Phys. Rev. Lett. **94**, 147602 (2005).
[12] N.J. Ramer, S.P. Lewis, E.J. Mele, *et al*., Fundamental Physics of Ferroelectrics 1998, Fifth Williamsburg Workshop, edited by R.E. Cohen. (American Institute of Physics, Melville, New York, 1998).
[13] N.J. Ramer and A.M. Rappe, Phys. Rev. B Rapid Comm. **62** 743 (2000).
[14] I. Grinberg, V.R. Cooper and A.M. Rappe, Nature **419**, 909 (2002).
[15] I. Grinberg, V.R. Cooper and A.M. Rappe, Phys. Rev. B **69**, 144118 2004
[16] P. Juhas, I. Grinberg, A.M. Rappe, *et al*., Phys. Rev. B **69** 214101 (2004).
[17] I. Grinberg and A.M. Rappe, Phys. Rev. B **70** 220101 (2004).
[18] Y.-H. Shin, V.R. Cooper, I. Grinberg, *et al*., Phys. Rev. B **71**, 054104 (2005).
[19] I. Grinberg and A.M. Rappe, Appl. Phys. Lett. **85** 1760 (2004).
[20] I. Grinberg, M.R. Suchomel, P.K. Davies, *et al*., J. Appl. Phys. **98** 094111 (2005).
[21] R.D. Shannon and C.T. Prewitt, Acta Cryst. Sec. B **26**, 1046 (1970).
[22] I.D. Brown, in *Structure and Bonding in Crystals II*, edited by M. O'Keeffe and A. Navrotsky (Academic Press, New York, 1981)
[23] M. Itoh, R. Wang, Y. Inaguma, *et al*., Phys. Rev. Lett. **94**, 3540 (1999).
[24] G.W. Watson, S.C. Parker and G. Kresse, Phys. Rev. B **59** 8481 (1999).
[25] U.V. Waghmare, N.A. Spaldin, H.C. Kandpal, *et al*., Phys. Rev. B **67** 125111 (2003).
[26] Z. Wu and R.E. Cohen, Phys. Rev. Lett. **95** 037601 (2005).
[27] P.K. Davies, Curr. Opin. Sol. Stat. and Mater. Sci., **4** 467 (1999).
[28] M.A. Akbas and P.K. Davies, J. Am. Ceram. Soc. **83** 119 (2000).
[29] E. Cockayne and B.P. Burton,Phys. Rev. B **60** 12542 (1999).
[30] R. Fisch, Phys. Rev. B **67** 094110 (2003).
[31] P. Juhas, M.A. Akbas and P.K. Davies, J. Am. Ceram. Soc. **87** 2086 (2004).
[32] M.R. Suchomel and P.K. Davies, Appl. Phys. Lett. **86** 262905 (2005).
[33] S.C. Abrahams, S.K. Kurtz and P.B. Jamieson, Phys. Rev. **172** 551 (1968).
[34] T. Egami, E. Mamontov, W. Dmowski, *et al*., in *Fundamental Physics of Ferroelectrics 2003*, edited by P.K. Davies and D.J. Singh (American Institute of Physics, Melville, New York 2003).
[35] J. Junquera and P. Ghosez, Nature **422**, 506 (2003).
[36] N. Sai, A.M. Kolpak and A.M. Rappe, Phys. Rev. B **72** 020101 (2005).
[37] D.D. Fong, A.M. Kolpak, J.A. Eastman, *et al*., Phys. Rev. Lett. **96** 127601 (2006).
[38] J.E. Spanier, A.M. Kolpak, J.J. Urban, *et al*., Nano Lett. **75** 735 (2006).
[39] C.H. Ahn, K.M. Rabe and J.-M. Triscone, Science **303** 488 (2005).